Shahid Beheshti University

Multiple-scale temporal variability of climatic time series in the western region of Iran

Abolfazl Neyestani [*]

Department of Physics, Razi University, Kermanshah, Iran

A B S T R A C T

The current research aims to carry out a multi-timescale variability analysis for the time series of sunspots (SN) precipitation (P_r) and maximum temperature (T_{max}) in four main stations in the western area of Iran. In addition, the emphasis is on the impact of the decadal solar cycle on the variability of climatic quantities. Appropriate statistical methods were employed to investigate the relationships between reconstructed time series. The results demonstrated that the more intense intra-annual to inter-annual fluctuations of the SN signal are synchronized with the peak of the decadal component of sunspots. For the monthly precipitation, the deviation from the regular yearly pattern is markedly related to intense intra-annual variations in comparison to the inter-annual plus decadal variations. While the dominant mode of variability of the SN, which contains 89% of the variance, occurs at low friquencies according to cumulative spectral power (CSP), the contribution of this band in the variability is less than 10% for the P_r and is trivial for the T_{max}. The result of wavelet coherence (WTC) analysis indicates a close connection between the variability of T_{max} and P_r at different timescales over the region, except for the 32-128-month scale, which is free of significant common oscillations. Furthermore, a signature of a significant decadal fluctuation was also observed between T_{max} and P_r which shows a completely different phase relationship for this timescale when compared to all smaller scales.

1. Introduction

Many climatic processes exhibit extreme variability, which may be on daily, seasonal, or year-to-year time scales. Thus, the variability of climatic data occurs on many temporal scales, but some timescales are more significant than others and thus involve more spectral density (Mitchell, 1976; von der Heydt et al., 2021). For instance, the temperature would vary over a wide range of timescales, from a few minutes to daily, monthly, annual, and even multi-decadal to millennial scales. Therefore, identifying dominant variability scales of terrestrial atmosphere data

and finding significant cyclical behaviors in the related signals are crucial, as well as other statistical moments, in statistical weather and climate forecasting. Air temperature and precipitation are the most fundamental elements for describing the climate and their variabilities can influence some important quantities such as humidity and hydrological variables (Peixoto and Oort, 1992; Tsiropoula, 2003; Zhang et al., 2019). Therefore, examining their oscillations in different timescales and finding any possible relationship between these two fundamental variables is of great importance. Information about the variability of temperature and

Precipitation is crucial since an understanding of their characteristics is extremely important for decision-making in the fields of water resources management, agricultural planning, economic and energetic issues, and determining the current and future climatic changes (Neukom et al., 2010; Jakob and Walland, 2016; Pendergrass et al., 2017). On the other hand, various external and internal climate forcings modulate these quantities. Temperature is affected by the action of a complex combination of terrestrial elements that can be controlled by numerous factors, including individual solar–astronomical components (Scafetta, 2014). In addition, precipitation time series also show highly complex behavior and thus have a noisy and erratic nature (Unnikrishnan and Jothiprakash, 2018; Neyestani et al., 2022). However, the description of precipitation characteristics and their prediction is of high climatological interest (Unnikrishnan and Jothiprakash, 2018, Pham et al., 2020; Yilmaz et al., 2021; Fahad et al., 2023). One of the most important external forcings impacts on atmospheric data is the change in the intensity of solar radiation. In addition to the fact that each latitude receives a specific amount of radiation during the year due to various astronomical and terrestrial factors, which leads to the variability in many meteorological quantities, other variabilities due to solar activities have been identified in the climate system (Roy and Kripalani, 2019). These activities can have significant effects on the spectral characteristics of incoming solar radiation (insolation) and consequently can cause other atmospheric variables to be influenced (i.e. natural climate variability). Indeed, the incoming solar radiation provides the energy budget for the earth and acts as the external driving for the earth-atmosphere system. The terrestrial factors such as clouds also have substantial effects on the incoming and outgoing radiation (Arking, 1991). There are several pieces of evidence from the scientific literature that show the solar influence on the atmospheric variables in different parts of the world over varying timescales (Xu and Powell, 2013; Thieblemont et al., 2015; Zhai, 2017; Sfica et al., 2018; Ogurtsov et al., 2020; S et al., 2022). The emphasis of these investigations is on the impact of the variability of sunspots on precipitation and temperature. For instance, Sfica et al. (2018) examined the solar influence on eight climatic parameters

recorded in Romania during 1961–2013 which corresponds with four cycles of sunspots. They found a weak solar influence with a clear spatial pattern, especially during the cold season, on temperature and cloud cover. Due to the extreme variability of sunspots in an approximately 11-year cycle, investigating their possible effects on atmospheric variables, especially at the same frequency, has received much attention. Nevertheless, assessing to what extent the 11-year solar cycle affects these variables has been a controversial issue and more clarification is required. Some researchers have claimed the insignificant impact of sunspots on the climate (Gil-Alana et al., 2014; Aparicio et al., 2020) and others have found some significant signatures (Laurenz et al., 2019; Zhang et al., 2021). Thus, there is no consensus about the possibility of a significant relationship between sunspot numbers and global atmospheric variability and additional investigations are required to improve our present knowledge. According to satellite data, total solar irradiance (TSI) varies by about 0.1% during each 11-year solar cycle between each solar minimum and solar maximum (Frohlich and Lean, 2004). Thus, direct and indirect cooling and warming of the Earth's surface and its atmosphere might somewhat be due to the changes in the number of sunspots. However, the variation of TSI during a solar cycle is trivial to directly trigger considerable impact on long-term climate variability (Svensmark and Friis-Christensen, 1997). Hence other indirect physical mechanisms can be responsible for possible significant impacts proposed in the scientific literature (Haigh, 1996; Svensmark and Friis-Christensen, 1997; Meehl et al., 2009; Svensmark et al., 2016). In addition, the role of clouds in energy balance is of high importance. The global coverage of clouds can be observed and gathered by satellites, and according to the recent studies, the global cloudiness can varied during the solar cycle due to the change in cosmic ray flux (Audu and Okeke, 2019). The variation in cloud cover due to 11-year solar activity can have a significant effect on the radiation balance and insolation. As a result, indirect effects such as the change in global cloudiness and the dynamics of general circulation pattern play a major role in the special distribution of the atmosphere's responses to solar variability (Kumar et al., 2023). The suggested changes in cloud covers due to solar activity are associated with changes

in rainfall and temperature (Audu and Okeke, 2019). Even though solar-induced changes because of the sunspots in global mean air surface temperature may be relatively small, regional and seasonal temperature changes associated with solar variability can be significant (de la Casa and Nasello, 2012). In addition, the variability of sunspots is not limited to the 11-year and the number of sunspots changes in different timescales. However, the 11-year oscillation is the main cyclical feature in the sunspots, which includes a large part of the variance. Besides solar variabilities, other usually more effective factors influence the surface climate, which obscure the solar signal and complicate its study (Gruzdev et al., 2019). For instance, the El Nino–Southern Oscillation (ENSO), volcanic eruptions, the quasi-biennial oscillation (QBO), and nonlinearity of processes that are responsible for solar-terrestrial connections could have a substantial effect (Ogurtsov et al., 2020). The issue under investigation in this paper deals with the following questions: 1. Can we obtain a noticeable and significant relationship between the precipitation and temperature data at different timescales? 2. Is there a significant relationship between the multiscale variations of sunspots and the variabilities in the precipitation and temperature on a regional scale? Thus, this study not only considers multi-timescale variations in the temperature and precipitation but also aims to collaborate on the debate regarding the influence of solar variability on precipitation and temperature. In the following, we have elucidated the temperature and precipitation variability and then have concentrated on the solar impact at regional scales based on analyses of precipitation and temperature recorded in the main stations over western Iran during 1979–2021. The study area and the datasets are described in section 2. In section 3, the methods of analysis and their implementations are fully explained. Time variations of co-variabilities are studied through the wavelet coherences and described in Section 4. For further consideration, other statistical methods such as correlation and spectral analyses are applied to the time series, and the results are presented in section 4. The results are discussed in section 5, and some conclusions of our statistical results are summarized in section 6.

2. Material and Methods

2.1. *Study area and datasets*

The study area is located in the western part of Iran. It extends between 34° and 36° North latitudes and 47° and 49° East longitudes (Fig. 1). This area is located in the central part of the Middle East, which is very vulnerable to facing climate change effects (Mansouri Daneshvar et al., 2019). In addition, the topography of the selected area is very complex, which can impose other constraints in the variability of the climatic time series. Four main stations with long-term data are selected for the analyses, including Kermanshah, Sanandaj, Khorramabad, and Hamedan. Monthly values of precipitation and maximum temperature over this area, provided by the Iran Meteorological Organization (IRIMO), were used in this study. By using monthly maximum temperature instead of monthly mean (minimum) temperature, we supposed that the impact of solar variability is more pronounced in maximum temperature rather than minimum temperature. The period of analysis consists of 42 years, starting from January 1979 and ending in December 2020. The raw data is normalized using the Z-score normalization method (section 3.1).

Fig. 1. The distribution of the selected stations over the western part of Iran

Monthly sampling values and the short length of the statistical period restricted us to only studying well-resolved variabilities. Thus, all variabilities between 2 to 143 months were extracted from the time series and studied. Precipitation and temperature time series, as with any tropospheric parameter, have a pronounced annual variation in this area (dominant mode of variability). Therefore, we carry out this investigation for the intra-annual (2-9 months), annual (9-18 months), and inter-annual plus decadal (18-143 months) bands. Statistical characteristics of the precipitation

(P_r) and maximum temperature (T_{max}) for the selected stations are described in Table 1. Monthly sunspot data (SN) were obtained from the World Data Center for the Production, Preservation, and Dissemination of the International Sunspot Number (https://www.sidc.be/silso/datafiles) for approximately four solar cycles, which correspond to the study period. The monthly sunspot data are also normalized according to the procedure used for the atmospheric data. The average monthly values of sunspots during the study period is 86, and its maximum is 284.

Table 1. Summary of the statistical information for selected stations during the period 1979-2021.

Station name	Latitude (°North)	Longitude (°East)	Elevation (m)	Average annual precipitation (mm)	Average annual maximum temperature (°C)	Standard deviation of precipitation (mm)	Standard deviation of maximum temperature (°C)
Kermanshah	34.32	47.08	1350	35.3	23.4	40.9	10.8
Sanandaj	35.31	46.99	1538	35.1	22.2	38.6	11
Khorramabad	33.46	48.33	1147	40.9	25.2	48.6	10.3
Hamedan	34.7	48.51	1850	26.3	19.7	28.3	11

2.2. Methods of analyses

2.2.1. Z-score normalization

First, we standardized the raw (original) data by employing the Z-score normalization technique. The Z-score normalization refers to the process of normalizing every value in a dataset such that the mean of all of the values is zero and the standard deviation is one. This procedure is a linear transform, which does not change the shape of the data distribution. The Z-score is computed straightforwardly according to the following equation (Han et al., 2023; Wilks, 2019):

$$z = \frac{x - \bar{x}}{S_x} \tag{1}$$

where x is the raw data, $\bar{x}$ is the average and S_x is the sample standard deviation for the entire period. The normalization makes it simple to evaluate fluctuations of different data sets if they have different means and standard deviations. The idea behind the standardization is to try to remove the influences of location and spread from a data sample. The physical units of the original data cancel, so standardized anomalies are always dimensionless quantities. The aforementioned standardization was applied for the SN, T_{max} and P_r signals, separately. This transform helps to remove the zero frequency component of the data in the frequency space, which means the constant mean of the data is not included in the produced

data. Subsequently, Lanczos low-pass, band-pass, and high-pass linear filters (Duchon, 1979) are used to isolate and study the different frequency bands of the time series. The standardized time series are broken down into three spectral bands by the linear filter. The first band (Band-1: 2-9 months) corresponds to intra-annual (sub-seasonal) fluctuations, and the second band (Band-2: 9-18 months) is indicative of annual variation to a large extent. The third band (Band-3: 18-143 months) is extracted from the data to be representative of inter-annual plus decadal fluctuations (i.e. longer-term variability: low-frequency component). Due to the monthly sampling time between each value, it is not possible to reveal the variabilities and their intensities for scales shorter than two months. In addition, the length of the data (42 years corresponds to 504 months) is another restrictive factor on the signal processing, which causes uncertain identification of the variabilities for longer timescales in the time series, for instance, inter-decadal and centennial scales. Thus, all the unclear variabilities at longer timescales than the decadal scale were filtered out to produce reconstructed signals before the spectral analysis.

2.2.2. Cumulative Spectral Power

A compact way of presenting fluctuations of some observation over different temporal scales

is through a power spectral density (PSD) (von der Heydt et al., 2021). The sharper peaks in the PSD diagram are straightforwardly interpreted and tend to be associated with frequencies in external quasi-periodic forcing related to the monthly, yearly, and longer or shorter periods. The broader peaks in turn often involve physical mechanisms within the climate system that vary on "typical" timescales but not on a well-defined period. Overall sharper and broader peaks exhibit preferred frequencies in the atmospheric time series, namely specific modes of climate variability. Furthermore, the continuous background spectrum is also considered. The PSD method can be unsuitable for time-varying noisy signals (Peters, 2007). As a solution, Cumulative Spectral Power (CSP) can be used to overcome some of the limitations of PSD (Neyestani et al., 2022). The CSP is similarly related to the PSD as the cumulative probability function (CPF) is constructed from the probability density function (PDF) in statistics. In other words, the CSP can be calculated by integrating the PSD function in the frequency domain. Since different fluctuations appear in climatic signals, integration of the PSD decreases the influence of the underlying noises in the frequency domain while preserving the essential information in a much more noticeable way. In the current study, the PSDs and CSPs for the reconstructed signals were computed, and some dominant components of variability were found in the related curves, along with their relative power.

2.2.3. Lagged Correlation

The correlation coefficient, r, is a way to determine how well two datasets co-vary linearly in time or space. For two random variables x (x_1, x_2, …, x_N) and y (y_1, y_2, …, y_N), the correlation coefficient (also known as the Pearson correlation) can be written as (Thomson and Emery, 2014):

$$r = \frac{C_{xy}}{s_x s_y} \tag{2}$$

where C_{xy} is the covariance of the x and y series, which is defined by:

$$C_{xy} = \frac{1}{N-1}\sum_{i=1}^{N}(x_i - \bar{x})(y_i - \bar{y}) \tag{3}$$

where s_x and s_y are the standard deviations, and $\bar{x}$ and $\bar{y}$ are the sample mean for the two data records. The degree of correlation in the datasets provides a way of roughly estimating the number of degrees of freedom within a given set of observations. The Pearson correlation as a global measure can be

calculated between each pair of observations at different time lags (i.e. lagged correlation). A lag of "m" means that the first m values of one of the series, say the y series, are removed so that y_{m+1} becomes the new y_1 and so on (Thomson and Emery, 2014). If a meaningful relationship exists between the two variables, it could be understood from the high correlations between them at a specific time lag (shift). In this study, the correlation coefficients at successive lags are calculated in order to find the possible significant relationships.

2.2.4. Wavelet coherence

The wavelet coherence (WTC) analysis is used to find the common scale-dependent fluctuations for (nonstationary) climatic time series in the time-frequency space (Roushangar et al., 2018). This method is especially useful in determining the time and scale intervals where two phenomena have a substantial interaction (Velasco and Mendoza, 2008). A squared wavelet coherence estimator (Addison, 2017; Torrence and Webster 1999) is defined as follows:

$$WCH_{g,h}^2(a,b) = \frac{\left|\langle T_g^*(a,b)T_h(a,b)\rangle\right|^2}{\langle|T_{g(a,b)}|^2\rangle\langle|T_h(a,b)|^2\rangle}$$

(4)

where 'g' and 'h' are a pair of sample time series, and the '*' indicates the complex conjugate of the continuous wavelet transform (CWT) for one of the time series. The $\langle\rangle$ symbol represents a localized smoothing operation in both time and scale performed on the constituent transform components. $T(a,b)$ shows the CWT at the scale and location parameters a and b, respectively, which is given by (Addition, 2017):

$$T_x(a,b) = \int_{-\infty}^{+\infty} x(t)\Psi_{a,b}^*(t)dt$$

(5)

Equation 5 contains both the time series, $x(t)$, and the conjugate of the dilated and translated mother wavelet, $\Psi^*((t-b)/a)$. The Morlet complex mother wavelet is used in climate studies because it provides a good balance between time and frequency localization (Torrence and Compo, 1998; Grinsted et al., 2004). This mother wavelet can be shown as:

$$\Psi(t) = \frac{1}{\pi^{\frac{1}{4}}}e^{i2\pi f_0 t}e^{\frac{-t^2}{2}} \tag{6}$$

According to equation 6, the Morlet mother wavelet is a complex wave within a Gaussian envelope and f_0 is the central frequency of the mother wavelet. The mother wavelet can be transferred to different locations on the time

series. In addition, it can be stretched and squeezed. Hence, one can compute the CWT along the time series and for different scales of the wavelet, through Eq. (5). Since the data were used are monthly data, the parameters for the CWT analysis were set as δt = 1 month (sampling time between each value), $a_0 = 2\delta t$ = 2 months (minimum scale of the wavelet), δj = 0.1 (octaves per scale), and maximum scale sets to 144 months. Hence, scales continuously ranged from two up to 144 months. The value of f_0, which is the frequency localization, was also chosen to be 6 for the Morlet wavelet for a better balance between time and frequency localization.

3. Results and discussion

3.1. Time series and their power spectra

The reconstructed time series based on the three spectral bands (from intra-annual to decadal) for sunspots (SN), maximum temperature (T_{max}), and precipitation (P_r) during the study period are presented in Figs. 2-4, respectively. This representation enables us to compare the variability of the selected parameters at different temporal scales. The prominent low-frequency variability is the main feature of the SN signal, and other fluctuations are relatively weak (Fig. 2a). The intra-annual variability (Band-1) is considerable when the solar activity is the greatest (i.e., solar maximum) compared to the years of solar minimum (Fig. 2b). The magnitude of the annual variability (Band-2) becomes larger when the sunspot numbers are maximum, similar to the intra-annual variability but with less intensity (Fig. 2c).
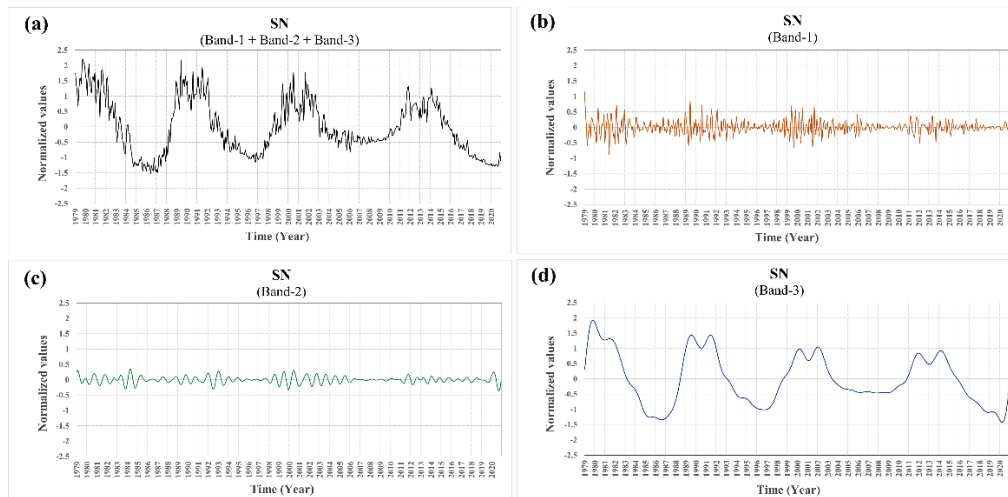

Fig. 2. Normalized time series of for the monthly sunspots data during the period 1979–2021: (a) The constructed SN signal contains all frequency components, from intra-annual to decadal, (b) Intra-annual fluctuations of SN, (c) Annual fluctuations of SN, and (d) Inter-annual plus decadal fluctuations of SN.

In other words, not only the solar-maximum years are indicative of the maximum of the 11-year component of solar cycle, but also, they are prone to intensify the solar variabilities in all smaller timescales. As shown in Fig. 2d, the most apparent feature of the SN signal is a dominant 11-year cycle with a double-peaked structure at Band-3 (i.e., inter-annual plus decadal scales). This structure at the solar-maximum years can originate from the pronounced inter-annual variability during the solar-maximum years in which solar activities are considerable. The magnitude of the fluctuations in the intra-annual, inter-annual plus decadal bands for the T_{max} is fairly small, compared with the magnitude of the original

signal (Fig. 3b-d and Fig. 3a). Meanwhile, the annual component is highly robust and regular (Fig. 3c) and hence has a substantial impact on the behavior of monthly temperature series (Fig. 3a). The relative magnitude of the intra-annual fluctuations displays a substantial variability in the precipitation time series in all years, especially in 1985 and 1995 (Fig. 4b). The annual component of precipitation, which is the main component of the precipitation variability in the western part of Iran, is inversely associated with the maximum temperature at the same timescale (Fig. 4c and Fig. 3c). It clearly shows that the highest precipitation amount due to the annual cycle occurs in the cold season. However, the intensity of the

precipitation fluctuations in this cycle is subject to noticeable variations than in the temperature in different years. Furthermore, the monthly precipitation fluctuations cover a broader range of effective timescales compared to the temperature that has relatively predictable behavior on an annual basis. More systematic variability for T_{max} can make it a potential candidate for predicting the general monthly precipitation behavior according to temperature variations at different timescales. Compared with the P_r, the contribution of intra-annual, inter-annual plus decadal variabilities (Band-1 + Band-3) in reconstructing the T_{max} signal is rather trivial.
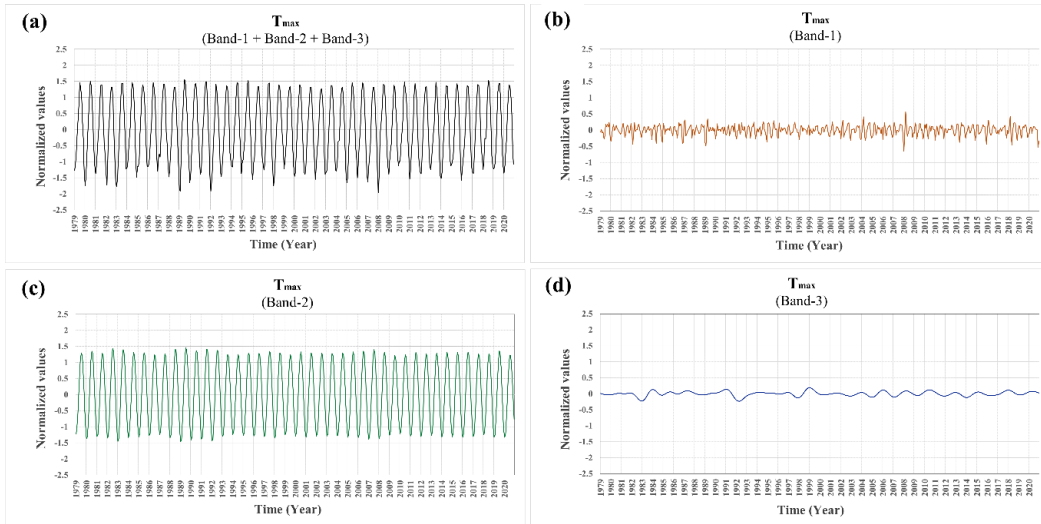

Fig. 3. As Fig. 2., but for the maximum temperature.
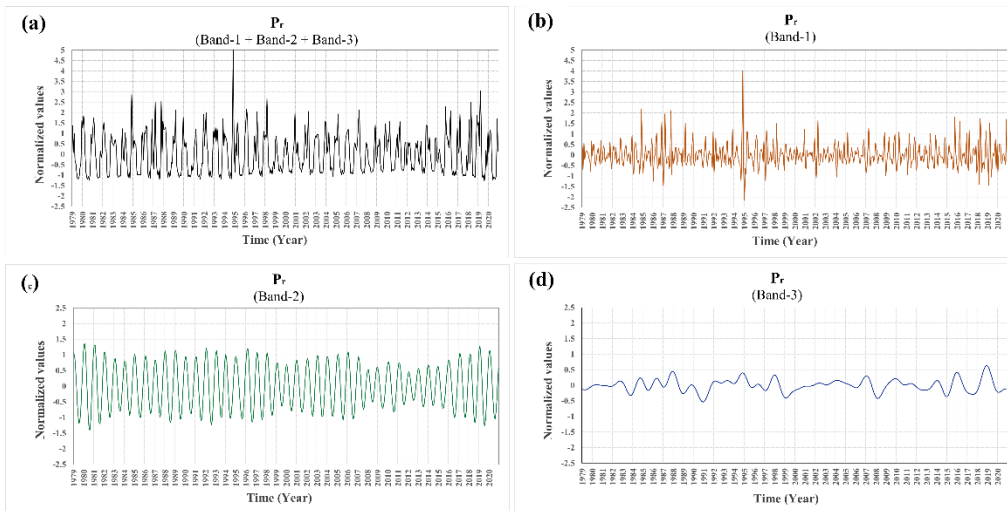

Fig. 4. As Fig. 2., but for the precipitation.

The power spectral density (PSD) for each time series is shown in Fig. 5. Generally, the power of the SN signal is considerable at 0.008 cpm (corresponds to approximately 10.5 years). This high spectral peak is significant at a 5% significance level. Furthermore, the magnitude of the fluctuations is higher at low and intermediate frequencies, but none of the spectral peaks except the 11-year peak are significant. In addition to the annual significant peak at Band-2 for the T_{max}, another significant peak can be observed at 0.17 cpm, which corresponds to a 6-month periodicity. The power spectra for the precipitation show three significant peaks at 0.08, 0.17, and 0.25 cpm, which imply 12-, 6-, and 4-month periodicity, respectively. The insignificant fluctuations of P_r spread equally over the frequency range, with larger magnitudes in comparison to the same components in T_{max}. Fig. 6 exhibits the CSP diagrams for the reconstructed SN, T_{max}, and P_r signals. As mentioned in the previous section, only the variabilities between 2-143 months were employed to estimate the variances of the

estimated signals in the frequency space. These curves show how the variance of each data series is distributed over the frequency range (harmonics). In addition to dominant scales of variability, possible periodicities can be found by precisely tracking the significant changes in the slopes between the adjacent harmonics. It should be noted that the CSP values are normalized (by the variance of each signal) and then multiplied to 100 to express the resulting values in percent (%). As can be seen in Fig. 6, sharp variation in the slope at a specific harmonic reveals the possible periodic (or almost periodic) components, which the magnitudes show the relative power. Because of the cumulative nature of the CSP curves, estimating the relative power for each harmonic should be obtained by subtracting the value of a specific harmonic in the CSP diagram from the value of the preceding harmonic. Hence, lines with zero slopes (perfectly flat in the horizontal direction) between two consecutive harmonics denote no variability in the succeeding harmonic. Moreover, moderate slopes over narrow or broad ranges of successive harmonics can be related to quasi-periodic or completely stochastic fluctuations, respectively. For instance, the considerable change in slope of the CSP diagram for the SN signal at harmonic 4, 5, and 6 seems to be associated with robust quasi-periodic component (large and sudden change in the slope: marked by black points), which contain 77% of the SN signal's variane. The high-frequency components (intra-annual and annual: Band-1 and Band-2) merely cover 11% of the SN signal's variance and behave stochasticly with small amplitude oscillations (Figs. 6 and 7). Furthermore, the inter-annual

stochastic variations of SN are dominant between harmonics 6-17, corresponding to 29-84 months (contain 10% of the variance). For the P_r and T_{max}, the annual periodicities are evident with extremely sharp slopes (harmonic 41-43), which comprise 95% and 43% of the variabilities for the T_{max} and P_r, respectively. This familiar winter-summer cycle is forced by variations in sunlight from the (very close to perfect) periodic motion of the earth around the sun, which causes the season change. Other almost cyclical behaviors, but with small intensity, can be noticed around 6- and 4-month periodicities (harmonic 83-91 and harmonic 125-127, 5% and 4% of the variance, respectively) for the precipitation. The impact of the 6-month cycle is less clear for T_{max} relative to the P_r. Overall, the intra-annual, inter-annual, and decadal variabilities of monthly maximum temperature are trivial, with dominant stochastic natures, relative to the annual component (1% for Band-3 and 4% for Band-1). The variabilities of the precipitation (with dominant stochastic nature) are 6% (of the variance) for inter-annual plus decadal and 47% for intra-annual harmonics. In order to identify the possible relationship between the main cyclical component of SN and both P_r and T_{max}, low-frequency components at Band-3 are precisely considered at the bottom of Fig. 6. The sudden 1% increase in the slope of the CSP for the precipitation at harmonic 5 and 6 suggests a possible relationship between the SN and the P_r at the decadal scale with a similar periodicity. In addition, the normal change in the slope for T_{max} in this band can be associated with the solar activities at Band-3.
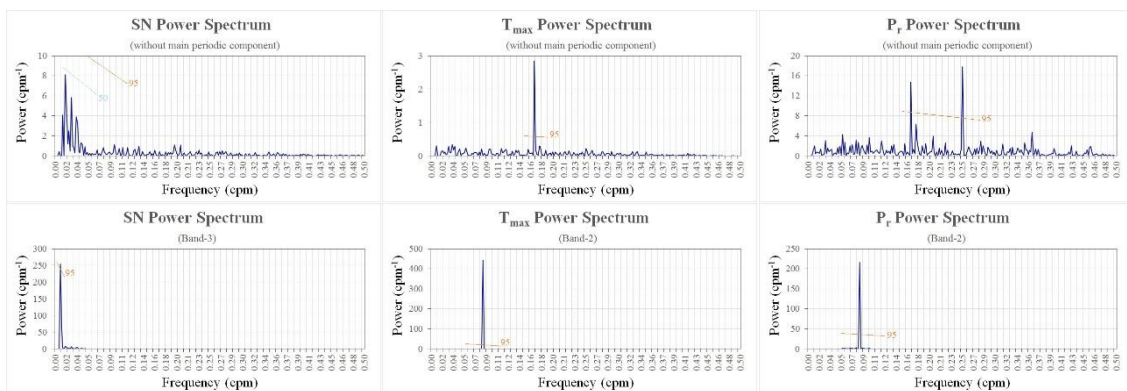

Fig. 5. Power spectral density (PSD) for the SN, T_{max} and P_r without taking into account the main periodic component (top) and for the frequency band that contains the main spectral peak for each signal (bottom).

Figure 7 represents the relative percentage of the different variabilities at three bands (Band-1, Band-2, and Band-3) from the total variance.

Approximately 90% of the SN variance stemmed from the decadal and inter-annual variabilities. For both the T_{max} and P_r, the intra-

annual variabilities are more effective than inter-annual and decadal variabilities, and the annual variabilities are the main component of the signals. Therefore, it can be concluded that the annual fluctuations of T_{max} and P_r largely determines the monthly precipitation and

temperature behavior in this region, without taking into account the inter-decadal and millennia variations (very low-frequency variations is not included in the reconstructed signals).
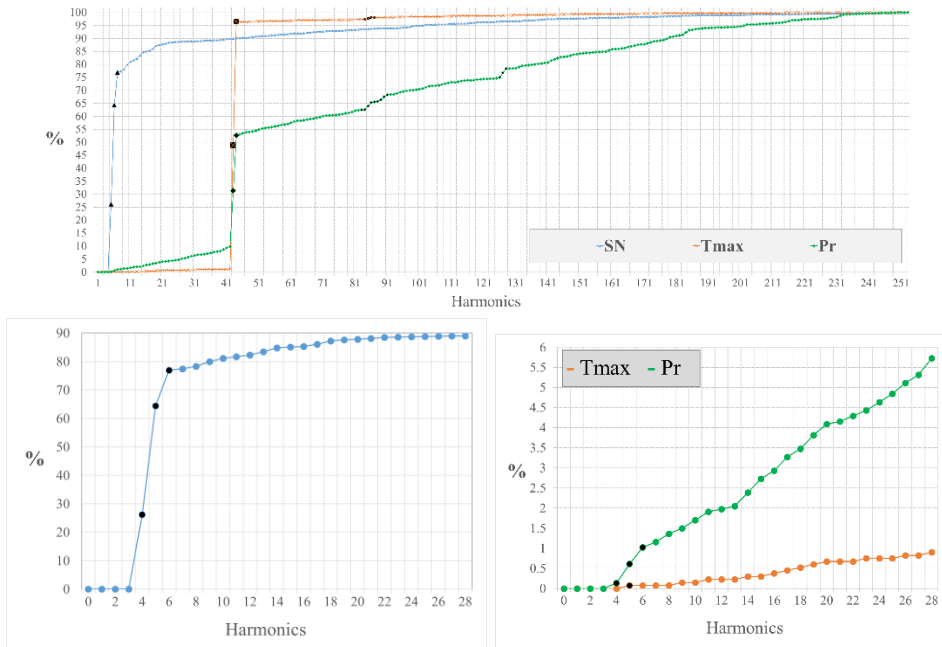

Fig. 6. Relative cumulative spectral power (CSP) (%) for the SN, T_{max}, and Pr time series. The harmonics less than 3 (corresponding to the periodicities greater than 12 years) are filtered out from the raw data because of the constraint imposed by the length of the time series. The largest harmonic (the component with highest frequency) corresponds to the two-month periodicity, which can be resolved from monthly data. The CSP for the harmonics less than 28 is displayed again at the bottom to reflect the effect of the 11-year solar cycle between harmonic 4-6 on T_{max} and P_r.
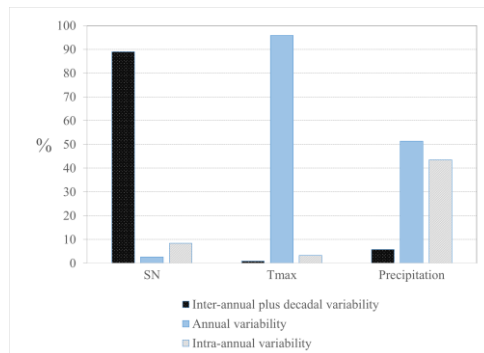

Fig. 7. The percentage of the variance for SN, T_{max} and P_r for different variabilities at different timescales.

For a thorough comparison, the decomposition of the variances for both T_{max} and P_r at each station is depicted in Fig. 8. Khorramabad station is more affected by the annual variabilities relative to other stations for both the T_{max} and P_r. Hamedan station is more under

the influence of intra-annual, inter-annual, and decadal fluctuations for both parameters. On the whole, due to the geographical proximity of stations, considerable differences were not observed.
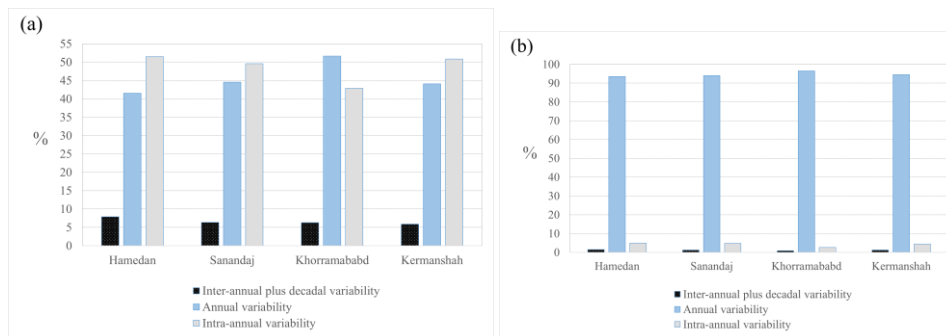
Fig. 8. A comparison among the relative intensities of variability at different timescales and for each station over the western part of Iran, (a) P_r, and (b) T_{max}.

3.2. Correlation analysis

Pearson correlation coefficient was used to measure the similarity between each pair of reconstructed signals (SN and T_{max}, SN and P_r, and also T_{max} and P_r) at different time lags. It demonstrates the strength of a linear relationship between the time series considering a range of time lags. The significance of the correlations was tested based on the two-tailed student's t-test at 95% confidence level. In order to explore the relationship between the sunspots and the selected atmospheric variables, the correlation coefficients were calculated from lag 0 to lag 150 (0-150 months). A wide range of lags was considered since a large variability of SN signal arises from the potent 11-year cycle (~ 132 months). The correlation analysis was carried out with three data series: 1. The reconstructed signals based on all constituent frequencies (2-143 months), 2. The low-frequency components of the data (Band-3), and 3. The reconstructed signals with filtering out the annual significant peak from the T_{max} and P_r signals. Considering all frequency components (Band-1 + Band-2 + Band-3), the cross-correlation coefficients are small (less than ±0.1) at different lags (Fig. 9a). However, these coefficients manifestly reflect the main periodicities in the SN, T_{max}, and P_r signals. The cross-correlation coefficients between the SN and T_{max} are insignificant for all lags. Meanwhile, the cross-correlations between SN and P_r are small but are significant at 95% confidence levels for some lags (lag 39-41 and 50-55). By only considering the inter-annual plus decadal components at Band-3, the cross-correlation coefficients increased compared to the situation with all frequency constituents in Fig. 9a (Fig. 9b). The correlation between SN and P_r reaches its maximum positive value (~ +0.35) at lag 54-57, and it is significant at a 95% confidence level (Fig. 9b). Meanwhile, the

correlation between SN and T_{max} drops to its (maximum) negative value (~ -0.35) at lag 32-34. Most of the correlations between SN and P_r, and also SN and T_{max} at different lags are statistically significant at a 95% confidence level for Band-3. Furthermore, the effect of the 11-year cycle of sunspots is clearly seen in the changes in the correlation coefficients with respect to the time lags for both temperature and precipitation, which have different phase relationships. The cross-correlation analysis for the SN-T_{max} and SN-P_r without considering the prominent annual cycle in the T_{max} and P_r signals indicates small and significant cross-correlation coefficients (Fig. 9c). It can be seen in Fig. 9c that the fluctuations of the cross-correlation function follow a similar pattern like the cross-correlation function in Band-3 (Fig. 9b), but with smaller correlation coefficients due to the inclusion of high- and intermediate-frequency components in the data. Table 2 indicates the correlation between the reconstructed T_{max} and the P_r series for each station and for the whole area. Merely correlations at lag 0 are shown, and the behavior of correlation coefficients for other lags is described in the following (Figures not shown). Considering all temporal variabilities in each signal (all three frequency bands), the correlation coefficients are always large and negative at lag 0 and significant at a 5% significance level. Hence, the large negative values imply a linear inverse strong relationship between precipitation and maximum temperature. In addition, because of the powerful annual variations in both T_{max} and P_r, the correlation coefficients that are calculated for Band-2 are extremely large for all stations. More investigation demonstrated that the modulus of the correlation coefficient is the largest at lag 0 compared to other lags for Band-1 (intra-annual), Band-2 (annual), and also the main estimated signals (Band-1 + Band-2 +

Band-3). The calculated correlations for Band-1 and Band-3 are lower when compared to Band-2 (the annual component), but are always negative and significant at a 5% significance level in all three bands at lag 0. Among all stations, Khorramabad station has the highest negative correlations at Band-1 and Band-3. Moreover, the correlation coefficients at Band-

1, Band-2, and Band-3 oscillate between negative and positive values at subsequent lags with approximately 6-month, 12-month, and 26-32-month periodicity, respectively (Figures not shown). Generally, a dominant anti-phase relationship appeared between precipitation and maximum temperature at intra-annual, annual, and inter-annual scales.
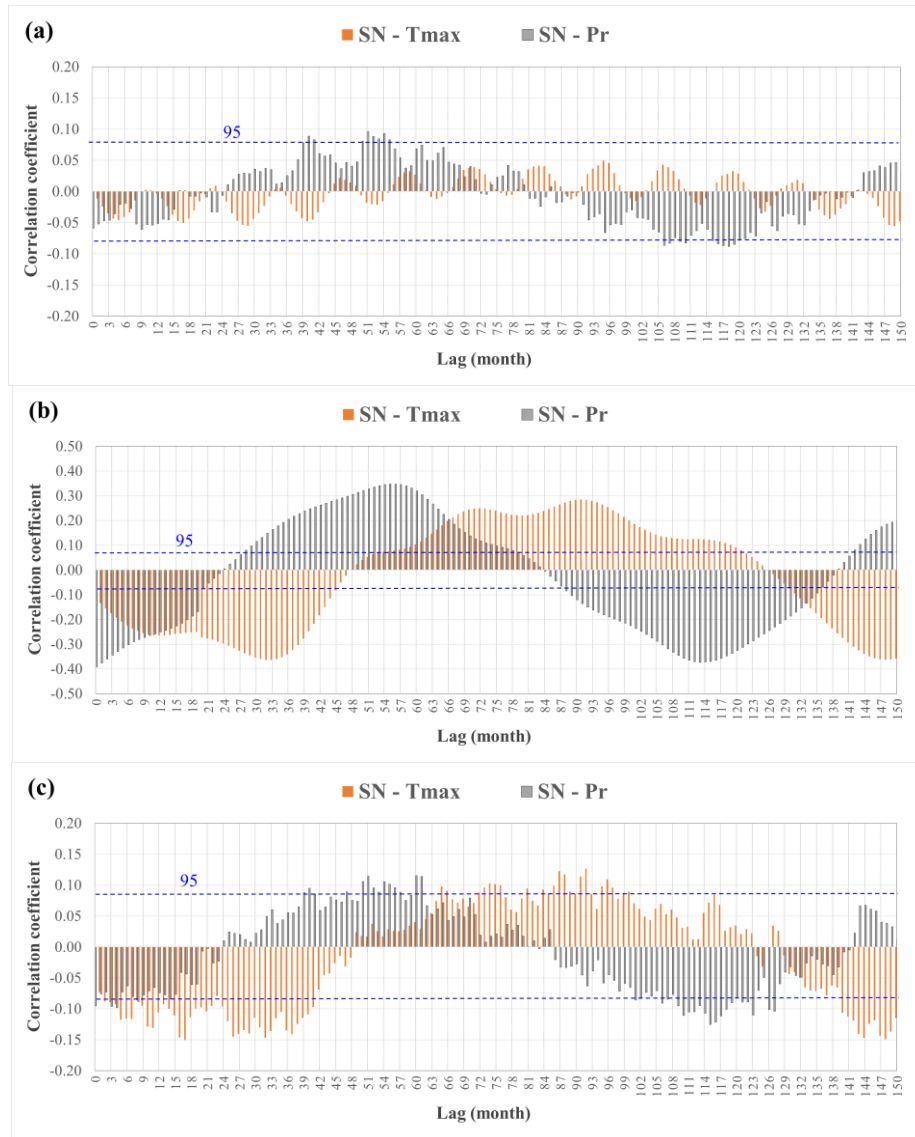

Fig. 9. Lagged cross-correlation for the SN-T_{max} and SN-P_r: (a) Considering all stochastic and periodic frequency components (Band-1 + Band-2 + Band-3) for SN, T_{max} and P_r, (b) Data at Band-3 (inter-annual plus decadal components), and (c) Considering all frequency components for SN, T_{max}, and P_r after filtering out the apparent annual cycle from the atmospheric data. The blue dashed lines show upper and lower confidence bounds at 95% confidence levels.

Table 2. Pearson correlation at lag 0 between maximum temperature and precipitation at confidence level of 95%.

	Total area	Kermanshah	Hamedan	Khorramabad	Sanandaj
All three bands	-0.74	-0.69	-0.64	-0.73	-0.67
Band-1 (intra-annual)	-0.34	-0.31	-0.27	-0.39	-0.26
Band-2 (annual)	-0.94	-0.93	-0.90	-0.93	-0.92
Band-3 (inter-annual plus decadal)	-0.43	-0.36	-0.29	-0.59	-0.33

3.3. Wavelet coherence analysis (WTC)

The wavelet coherence plots, which reveal the magnitude and phase of the coherences (or localized correlations) between the SN and P_r signals at different scales (periodicities), as well as changes in the correlation over time at every single station, are displayed in Fig. 10. The wavelet coherence spectrum for these series exhibits the presence of some significant annual, sub-annual, and inter-annual plus decadal coherences at each station. A collection of arrows was added to the high-coherence areas in the WTC plots, which shows the phase information regarding both time series. The right-pointing arrows indicate no phase shift between the SN and P_r (in-phase or synchronous relationship, which means the simultaneous occurrence of two phenomena). The left-pointing arrows display half of a period shift (anti-phase relationship). Furthermore, vertical up- (down-) pointing arrows imply that the SN is lagging (leading) with respect to the P_r for one full quarter of a period, which indicates an out-of-phase situation. Continuous black contours in the WTC plot, which surround the areas with high coherences, are indicative of the 5% statistical significance level for a red noise process. Furthermore, the light-shaded area outside the cone of influence (COI), which is under the influence of the edge effects, shows the region where the interpretation should be carried out with caution because of increased uncertainty. The arrows in the WTC plots are displayed to indicate the phase information only when the localized correlations are higher than 0.6. According to Fig. 10, the scale of 2–8 months (intra-annual variation) shows sporadic significant co-variability between the SN and P_r for all stations, in which the phase differences are variable (and therefore inconsistent) over time. On the other hand, as displayed in Fig. 7, only 9% of the variance of the SN signal is distributed in the intra-annual scale compared to approximately 42% for the precipitation. Thus, the direct effect of SN fluctuations at Band-1 on the P_r considering the whole statistical period can be negligible. Accordingly, due to inconsistent phase relationships, the co-variabilities at the 2-8-month band can be regarded as insignificant at different stations. Because of the high similarity between the annual variations of P_r at all stations, the coherences show relatively similar patterns

between SN and P_r at the 8-16-month band (Fig. 10). Some significant intermittent coherences at the 8-16-month scale are evident mostly at the solar-maximum years. However, the phase of the fluctuations is not the same during the study period, similar to intra-annual coherences. The most significant correlations can be found in 1998-2005 with dominant anti-phase relationships, which are concurrent with solar-maximum years with a considerable annual variation of sunspots (Fig. 4). The insignificant and weak annual co-variability after 2005 can be due to a weak 11-year solar cycle, and the corresponding small annual fluctuations of SN. The reversal of phases is visible at different times for the 8-16-month scale. Overall, the possible effect of the inter-annual component of sunspots (16-100 months) on the same scale of precipitation fluctuations is mostly insignificant except for a limited number of years and in specific frequency bands, and the co-variability of these quantities does not occur with a consistent phase relationship during different years. All four stations in the inter-annual band show different coherence patterns. The sporadic high localized correlations can be observed during 1984-1987 and 2011-2013 for Kermanshah at a scale of 16-32 months, during 1988-1994 in Sanandaj at a scale of 32-64 months, and during 1985-1989 in Hamedan at a scale of about 64 months. A stable decadal co-variability (128-month periodicity) with a permanenty anti-phase relationship is found between SN and P_r at all stations except for Hamedan. The WTC analysis between SN and T_{max} exhibits higher similarity among all stations when compared to the same analysis between SN and P_r over the frequency range, even in intra-annual (2-8 months) and inter-annual (16-100 months) scales (Fig. 11). The more pattern similarity for WTC plots of different stations for SN-T_{max} than for SN-P_r is due to the more comparable temperature variabilities (on different timescales) at nearby stations. There are generally significant co-variability patterns on timescales of less than four months in 1985, 1990, 1992, 1995, 1998, 2008, 2010 and 2013. Furthermore, significant coherences on a 6-month scale were found in a few years (1981, 1986, 1989 and 2013), with dominant anti-phase relationships in the high coherences areas. In the annual scale (8-16 months), significant localized correlations (with phase reversal) were observed for SN-T_{max}

similar to SN-P_r, but with an opposite phase relationship (Figs. 10 and 11). A more important feature at the inter-annual scale in the WTC plots in Fig. 11 is the significant co-variability of SN with T_{max} in the scale of 16-32 months between 2011-2015, with a phase difference of 180° which is also found in the wavelet coherence of the SN-P_r at Kermanshah station but with opposite phase (synchronous relationship, Fig. 10a). However, the high coherence areas is merely significant for Kermanshah, Sanandaj and Khorramabad stations at a 5% significance level, and is insignificant for Hamedan station. Another high coherence area with a phase difference of ~ 45° at this scale was found in 1989-1991, which is only significant in Khorramabad station at a 5% significance level. The WTC plots of SN-T_{max} show that at the decadal scale (~ 100-140 months), for all four stations, there is a stable fluctuation in the entire statistical period at a 95% statistical confidence level (Fig. 11, bottom of the plots). The phase difference displayed by the arrows is ~ 100-120°, and since the direction of the arrows is almost upward, the T_{max} is leading the SN with a phase difference of one-third of the period (3-4 years) on this scale. In other words, if the SN signal is considered as a cause and the T_{max} signal as the effect, the peak of the 11-year fluctuation in T_{max} has a phase delay of ~ 220-260° relative to the same peak in SN, which corresponds to ~ 7 years. Hence, the minimum value of the 11-year component of T_{max} occurs approximately 3-4 years after the maximum of this component in SN (consistent with the result of lagged correlation in Fig. 9b: negative correlation

around lag 36). However, it is noteworthy to say that despite the high and stable coherences, the T_{max} in the decade band contains trivial power compared to other bands (Figs. 7 and 8). Therefore, regardless of the high coherence between the SN and T_{max} in this band and the consistent phase relationship during all years, the effect of this localized high correlation on the variation of the maximum temperature at the selected stations and also on the (global) correlation between the two signals (including all frequency bands: Band-1 + Band-2 + Band-3) will be slight. Fig. 11 indicates the WTC between T_{max} and P_r values. Visual inspection showed apparent stable annual variability for both signals, in which the magnitude of the coherences are intensified in some years (extremely high localized correlation) and weakened to some extent in other years (relatively high localized correlation). In addition, the values of coherences in the 8-16-month band are substantial (greater than 0.8) in all stations during the period and fulfill the 5% significance criterion. These suggest a strong inverse relationship between T_{max} and P_r due to the annual cycle of solar radiation. Since the power of both signals at Band-2 is also considerable (Fig. 8: ~ 95% for T_{max} and ~ 40-50% for P_r), the impact of these common anti-phase fluctuations will be substantial on the (global) correlation between these two signals. Moreover, the simultaneous intensifying and weakening of the localized correlations at the annual scale during the study period imply that the same forcing drives this pattern for all four stations.
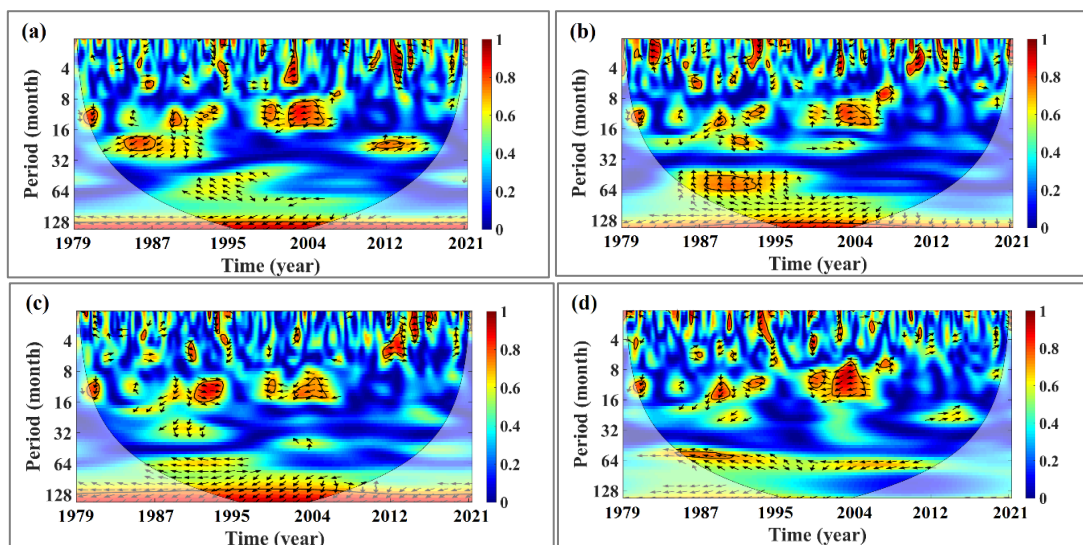

Fig. 10. Wavelet coherence (WTC) for the period 1979-2021, between the monthly sunspots and precipitation series for different stations: (a) Kermanshah, (b) Sanandaj, (c) Khorramabad (d) Hamedan.
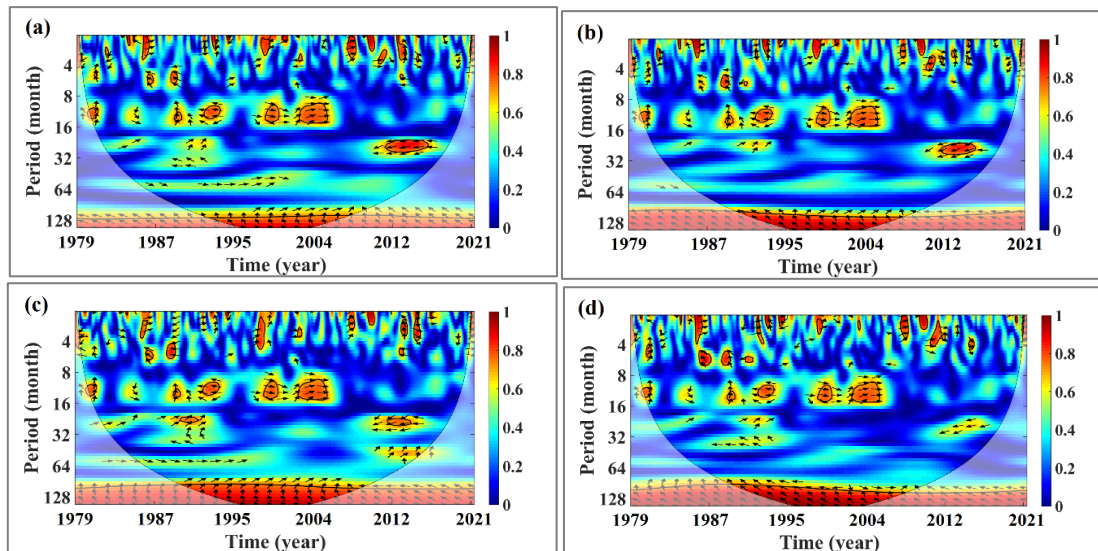
Fig. 11. Wavelet coherence (WTC) for the period 1979-2021, between the monthly sunspots and maximum temperature series for different stations: (a) Kermanshah, (b) Sanandaj, (c) Khorramabad (d) Hamedan.

In addition to significant annual co-variability, other high coherences are apparent at different periods (intra-annual, inter-annual, and decadal scales) in different time intervals (Fig. 12). Specifically, sporadic high coherences are evident in the intra-annual band with dominant anti-phase relationships for all stations. Furthermore, different significant inter-annual and decadal co-variabilities were found for all stations at specific bands. The main characteristic of these common fluctuations is their intermittency and the dominant anti-phase relationship. As is shown in Fig. 12, the main part of the common inter-annual fluctuations concentrates around the 24-to-32-month scale for Kermanshah and Sanandaj stations and around 24-to-64-month for Hamedan. Significant co-variability for the scale of 32-128 months in the T_{max} and SN signals is rare for Kermanshah, Sanandaj, Khorramabad, and also for the scale of 64-128 months for Hamedan. At the decadal scale at the bottom of the WTC plots, significant co-variability between T_{max} and P_r is noticed mostly at Hamedan station and to some extent at Kermanshah and Sanandaj stations. The phase difference indicates that the maximum of the decadal component of P_r occurs 3-4 years before the maximum of the same one of T_{max}.
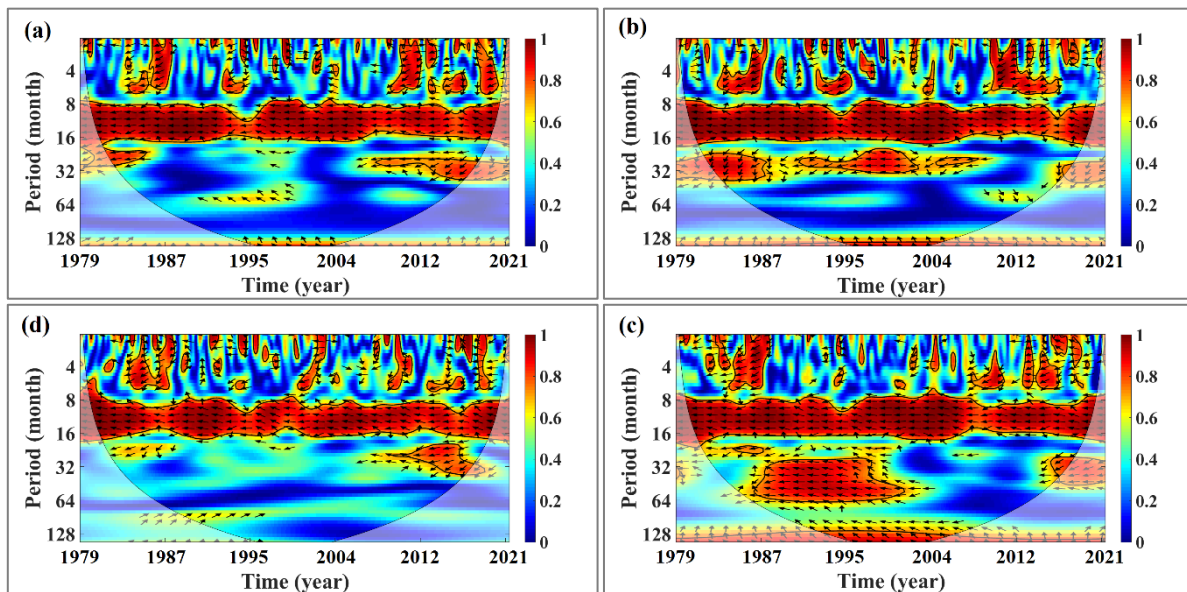

Fig. 12. Wavelet coherence (WTC) for the period 1979-2021, between the monthly maximum temperature and precipitation series for different stations: (a) Kermanshah, (b) Sanandaj, (c) Khorramabad (d) Hamedan.

The linkage between SN with P_r and T_{max}, and also T_{max} with P_r, is investigated in the whole extent of the western part of the country, in addition to the single stations. For this purpose, the T_{max} and P_r monthly values were averaged over four stations to obtain the relevant time series for each quantity (Figs. 3-4a) and then analyzed with the SN (Fig. 2a) to find common features. Figure 13 presents the WTC plots and shows an apparent 128-month reoccurrence pattern with a broader band for SN-T_{max} and a narrower band for T_{max}-P_r. The phase difference between the SN and P_r at the 128-month period is ~ -135° (Fig. 13a), which shows the SN decadal fluctuation precedes the P_r by 3-4 years. Furthermore, the phase difference for SN-T_{max} in the decadal band indicates that the SN signal is ahead by 6-7 years (Fig. 13b). For the T_{max}-P_r, the significant anti-phase co-variabilities are concentrated on the 2-8-month, 8-16-month, and 24-32-month periods (Fig. 13c). Furthermore, the influence of decadal significant common fluctuations (larger than 128-month period) is detectable (bottom of the plot).

3.4. Discussion

As ivestigated in this paper, the variability of atmospheric data covers a broad range of temporal scales. Other than preferred scales of the variability in maximum temperature, precipitation, and sunspots, the spectrum of each variable provides insight into the dynamics of the Earth system as a whole (von der Heydt

et al., 2021). In addition to the 'background spectrum', preferred frequencies like the sharp or flat peaks can be identified, which are set by specific modes of internal or external climate variability. All three statistical methods we used in this study can be regarded as complementary methods, and these methods are quite beneficial for elucidating long- and short-term variability contained in the precipitation, temperature, and sunspots time series. Using PSD and CSP methods revealed the major components and their relative intensities. Hence, applying these methods resulted in the identification of several dominant quasi-periodic peaks and underlying spectra in the frequency domain. The robust shorter period of one year corresponds to seasonal variations in the precipitation and temperature, typical for the continental stations of the Northern Hemisphere (Borkovic and Bronic, 2021). These findings suggest that using a spectral method like CSP is an appropriate way to study different temporal scales of the climatic time series and to identify the main deterministic and stochastic components. Furthermore, the relative importance of each component in reconstructing the time series can be recognizable through CSP. Therefore, the results suggest that the statistical modeling and prediction of climatic time series can be conducted by dividing the variability of the complex time series into their main deterministic and stochastic components, taking into account the background noises.
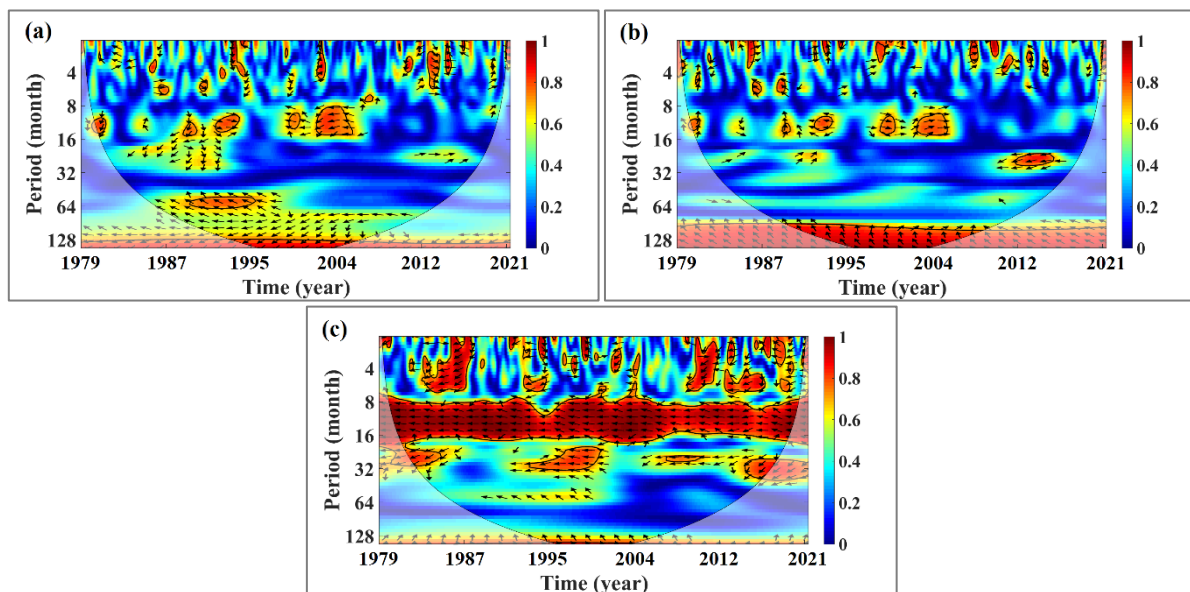

Fig. 13. Wavelet coherence (WTC) for the whole area during the period 1979-2021, (a) between the monthly sunspots and precipitation, (b) between the monthly sunspots and maximum temperature, (c) between the monthly maximum temperature and precipitation.

The relative impact of the 11-year solar cycle on the long-term variability of precipitation and temperature, which was quantified by CSP in this study, is also investigated by other scholars (Thomas et al., 2023; Neyestani et al., 2022; Ogurtsov et al., 2020; Laurenz et al., 2019; Sfîc et al., 2018) and similar results have been obtained. Thomas et al. (2023) used the wavelet transform to highlight the relationship between rainfall and sunspots over Kerala in India. The time series analysis showed common features at 8-18 years with varying significance. Neyestani et al. (2022) carried out research concerning the relationship between large-scale circulations and precipitation and temperature over Iran using re-analysis gridded data. They found that the surface temperature and precipitation variations are strongly linked together over the whole area of Iran, in particular at annual cycle. Their results also indicated a piece of evidence regarding the impact of the 11-year solar cycle on precipitation and temperature over Iran, which are consistent with the results of the current study in individual stations. The correlation analysis at successive time lags measured the amount of linearity between each pair of time series and hence used to show generally possible relationships. The wavelet coherences showed the scale-dependent common variability of sunspots, temperature, and precipitation over the period of 1979–2021. Accordingly, these two methods are capable of indicating the effect of 11-year solar activity on precipitation and temperature as a global (independent of time scales) or local (dependent on time scale) measure, which are employed by other authors in this field of study (Zhang et al., 2021; Laurenz et al., 2019). New analysis method like WTC aims to determine how fluctuation levels at each time scale are related. One interpretation of these results is that apart from phenomena directly attributable to an external forcing, such as the annual cycle in monthly atmospheric data, other variabilities, such as the effect of sunspots, have a very complex nature and can be considered as a part of the background signal (Lovejoy and Schertzer, 2013). The background signal originates from multifractal cascading processes such as those in turbulent flows. On the other hand, the revolution of the Earth around the Sun causes the annual forcing, and with the daily rotation, constitutes indubitably the most prominent spectral peak of most climatic variables. Compared with most typical time scales of climate variability that we considered here; the annual (seasonal) cycle is clearly on a rather short time scale. Nevertheless, it strongly interacts with many slower modes of variability; for example, inter-annual phenomena such as the El Nino-Southern Oscillation (ENSO) tend to be locked to the seasonal cycle (Rasmusson and Carpenter, 1982). Furthermore, it was indicated that the ENSO phenomenon is under the influence of solar activity during the 11-year solar cycle (Neyestani et al., 2022, Hassan et al., 2016, Fu et al., 2012).

Different statistical methods we employed in this study can somehow provide an increased contribution to unravel the complexity of the Sun–climate impact, especially regarding the stochastic components. Obviously, the direct impact of solar activity on the variability of climatic data is difficult to outline, due to the complex processes that occur in the Sun–Earth environment, taking into consideration the complexity of the climate system (Mares et al., 2021).

4. Conclusion

4.1. Concluding remarks

In this research, the variability of the precipitation, maximum temperature, and sunspots at different timescales from 2 to 143 months was studied for 42 years in the western part of Iran, which is very vulnerable to climate change. An assessment was carried out to quantify the intensity of variabilities at intra-annual, annual, and inter-annual plus decadal scales, represented by Band-1, Band-2, and Band-3, respectively. Our findings and conclusions can be summarized as follows:

1. All the considered signals have some dominant scales of variability. Due to the limited length of data and the monthly sampling, the variability analysis was confined to the 2-143-month. The dominant cyclic and stochastic behaviors were found concerning the variability of the data. For instance, periodic and almost-periodic components with considerable power were identified in the SN, T_{max}, and P_r by the PSD and CSP analysis, similar to the previous studies conducted by other scholars. 2. The lagged correlation analysis is a helpful method to distinguish the amount of linear relationship between two different time-dependent datasets. The Pearson

correlation coefficient was used at different time lags, from 0 to 150 months, to quantify any possible linkage between SN and the T_{max}, and also P_r, taking into account all frequency components and the inter-annual plus decadal component of the time series. Some pieces of evidence regarding the impact of the solar cycle (with a time delay) on precipitation and maximum temperature were found in the western part of Iran (see the correlation coefficients above 95% confidence level in Fig. 9b, c). However, the impact is not so powerful to have a large influence on the behavior of T_{max} and P_r in this area. 3. Applying the wavelet coherence approach to the signals generally shows continuous significant common oscillations with consistent phase relationships for the SN-P_r and SN-T_{max} in decadal periodicities. In addition, for the T_{max}-P_r all the fluctuations in the 2-6-month, 8-16-month, 24-32-month, and 128-143-month bands show intermittently or continuously significant coherences with a dominant anti-phase relationship throughout the mentioned scales and the study period. The decadal oscillation of P_r is somewhat more substantial than T_{max} in association with the SN. The impact of the solar cycle led to detectable variation in the P_r signal, which was confirmed by the lagged correlation analysis. Overall, the findings obtained in this study provide further insight into the temporal variation of precipitation and temperature, which are the main effective elements in managing the water resources and identifying climate change in the west of Iran. Furthermore, the current study attempted to contribute to the issue of solar-terrestrial interaction on a regional scale. The insights we obtain by the variability analysis are crucial for understanding different interactions in the climate system, and the approach used in this study can also be applied in other geographical regions and for other climatic quantities.

Acknowledgment

References

Addison, P.S., 2017. The Illustrated Wavelet Transform Handbook: Introductory Theory and Applications in Science, *Engineering, Medicine and Finance*. 2nd Edition, CRC Press.

Aparicioa A.J.P., Gallegoa, M.C., Antóna, M. & Vaquero, J.M., 2020. Relationship between solar activity and direct solar irradiance in Madrid (1910–1929). *Atmospheric Research*, 235, 104766.

Arking, A., 1991. The radiative effects of clouds and their impact on climate. *Bulletin of the American Meteorological Society*, 72, 795-813.

Audu, M.O. & Okeke, F.N., 2019. Investigation of possible connections between solar activity and climate change in Nigeria. *SN Applied Sciences*, 1, 149.

Borkovic, D. & Bronic, I.K., 2021. Solar activity cycles recorded in long-term data on tritium activity concentration in precipitation at Zagreb, Croatia. *Radiation Physics and Chemistry*, 188, 109646.

de la Casa, A.C. & Nasello, O.B., 2012. Low frequency oscillation of rainfall in Córdoba, Argentina, and its relation with solar cycles and cosmic rays. *Atmospheric Research*, 113, 140-146.

Duchon, C.E., 1979. Lanczos filtering in one and two dimensions. *Journal of Applied Meteorology and Climatology*, 18, 1016-1022.

Fahad, Sh., Su, F., Khan, S.U. et al., 2023. Implementing a novel deep learning technique for rainfall forecasting via climatic variables: An approach via hierarchical clustering analysis. *Science of The Total Environment*, 854, 158860.

Fröhlich, C. & Lean, J., 2004. Solar radiative output and its variability: evidence and mechanisms. *The Astronomy and Astrophysics Review*, 12, 273-320.

Fu, C., James, A.L. & Wachowiak, M.P., 2012. Analyzing the combined influence of solar activity and El Niño on streamflow across southern Canada. *Water Resources Research*, 48, W05507.

Gil-Alana, L.A., Yaya, O.S. & Shittu, O.I., 2014. Global temperatures and sunspot numbers. Are they related?. *Physica A: Statistical Mechanics and its Applications*, 396, 42-50.

Grinsted, A., Moore, J.C. & Jevrejeva, S., 2004. Application of the cross wavelet transform and wavelet coherence to geophysical time series. *Nonlinear Processes in Geophysics*, 11, 561-566.

Gruzdev, A.N. & Bezverkhnii, V.A., 2019. Analysis of solar cycle-like signal in the North Atlantic Oscillation index. *Journal of Atmospheric and Solar-Terrestrial Physics*, 187, 53-62.

Haigh, J.D., 1996. The impact of solar variability on climate. *SCIENCE*, 272(5264), 981-984.

Han, J., Pei, J. & Tong, H., 2023. Data Mining: Concepts and Techniques. 4th Edition, *Elsevier* Inc.

Hassan, D., Iqbal, A., Hassan, S.A. et al., 2016. Sunspots and ENSO relationship using Markov method. *Journal of Atmospheric and Solar-Terrestrial Physics*, 137, 53-57.

Jakob, D. & Walland, D., 2016. Variability and long-term change in Australian temperature and precipitation extremes. *Weather and Climate Extremes*, 14, 36-55.

Kumar, V., Dhaka, S.K., Hitchman, M.H. & Yoden, S., 2023. The influence of solar-modulated regional circulations and galactic cosmic rays on global cloud distribution. *Scientific Reports*, 13, 3707.

Laurenz, L., Ludecke, H.J. & Lunin, S., 2019. Influence of solar activity changes on European rainfall. *Journal of Atmospheric and Solar-Terrestrial Physics*, 185, 29-42.

Lovejoy, S. & Schertzer, D., 2013. The weather and climate: emergent laws and multifractal cascades. Cambridge University Press, First Cambridge Mathematical Library Edition, Cambridge, UK.

Mansouri Daneshvar, M.R., Ebrahimi, M. & Nejadsoleymani, H., 2019. An overview of climate change in Iran: facts and statistics. *Environmental Systems Research*, 8, 7.

Mares, C., Dobrica, V., Mares, I. & Demetrescu, C., 2022. Solar Signature in Climate Indices. *Atmosphere*, 13(11), 1898.

Meehl, G.A., Arblaster, J.M., Matthes, K. et al., 2009. Amplifying the pacific climate system response to a small 11-Year solar cycle forcing. *SCIENCE*, 325(5944), 1114-1118.

Mitchell, J.M., 1976. An overview of climatic variability and its causal mechanisms. *Quaternary Research*, 6, 481-493.

Neukom, R., Luterbacher, J., Villalba, R. et al., 2010. Multi-centennial summer and winter precipitation variability in southern South America. *Geophysical Research Letters*, 37, L14708.

Neyestani, A., Karami, Kh. & Gholami, S., 2022. Exploring the possible linkage between the precipitation and temperature over Iran and their association with the large-scale circulations: Cumulative spectral power and wavelet coherence approaches. *Atmospheric Research*, 274, 106187.

Ogurtsov, M., Veretenenko, S.V., Helama, S. et al., 2020. Assessing the signals of the Hale solar cycle in temperature proxy records from Northern Fennoscandia. *Advances in Space Research*, 66, 2113-2121.

Peixoto, J.P. & Oort, A.H., 1992. Physics of Climate. 1st Edition, American Institute of Physics.

Pendergrass, A.G., Knutti, R., Lehner, F. et al., 2017. Precipitation variability increases in a warmer climate. *Scientific Reports*, 7, 17966.

Peters, R.D., 2007. A new tool for seismology - the cumulative spectral power. *Mercer University Macon, Georgia,* online at http://physics.mercer.edu/hpage/CSP/cumulative.html

Pham, B.T., Le, L.M., Le, T.T. et al., 2020. Development of advanced artificial intelligence models for daily rainfall prediction. *Atmospheric Research*, 237, 104845.

Rasmusson, E.M. & Carpenter, T.H., 1982. Variations in tropical Sea surface temperature and surface wind fields associated with the Southern Oscillation/El Nino. *Monthly Weather Review*, 110, 354-384.

Roushangar, K., Alizadeh, F. & Adamowski, J., 2018. Exploring the effects of climatic variables on monthly precipitation variation using a continuous wavelet-based multiscale entropy approach. *Environmental Research*, 165, 176-192.

Roy, I. & Kripalani, R.H., 2019. The role of natural factors (part 1): addressing on mechanism of different types of ENSO, related teleconnections and solar influence. *Theoretical and Applied Climatology*, 137, 469-480.

S, A., T.E, G., V.G, H. et al., 2022. Amplitude modulation of sunspot cycles and its influence on monsoon rainfall variability and occurrences of major droughts in India. *Theoretical and Applied Climatology*, 149, 1419-1430.

Scafetta, N., 2014. Global temperatures and sunspot numbers. Are they related? Yes, but non linearly. A reply to Gil-Alana et al. (2014). *Physica A: Statistical Mechanics and its Applications*, 413, 329-342.

Sfica, L., Iordache, I. & Voiculescu, M., 2018. Solar signal on regional scale: A study of possible solar impact upon Romania's climate. *Journal of Atmospheric and Solar-Terrestrial Physics*, 177, 257-265.

Svensmark, J., Enghoff, M.B., Shaviv, N.J. & Svensmark, H., 2016. The response of clouds and aerosols to cosmic ray decreases. *Journal of Geophysical Research: Space Physics*, 121(9), 8152-8181.

Svensmark, H. & Friis-Christensen, E., 1997. Variation of cosmic ray flux and global cloud coverage – a missing link in Solar-climate relationships. *Journal of Atmospheric and Solar-Terrestrial Physics*, 59, 1225-1232.

Thieblemont, R., Matthes, K., Omrani, N.E. et al., 2015. Solar forcing synchronizes decadal North Atlantic climate variability. *Nature Communications*, 6, 8268.

Thomas, E., Joseph, I. & Abraham, N.P., 2023. Wavelet analysis of annual rainfall over Kerala and sunspot number. *New Astronomy*, 98, 101944.

Thomson, R.E. & Emery, W.J., 2014. *Data Analysis Methods in Physical Oceanography*. 3rd Edition, Elsevier Science.

Torrence, C. & Compo, G., 1998. A practical guide to wavelet analysis. *Bulletin of the American Meteorological Society*, 79, 61-78.

Torrence, C. & Webster, P.J., 1999. Interdecadal changes in the ENSO-Monsoon system. *Journal of Climate*, 12(8), 2679-2690.

Tsiropoula, G., 2003. Signatures of solar activity variability in meteorological parameters. *Journal of Atmospheric and Solar-Terrestrial Physics*, 65(4), 469-482.

Unnikrishnan, P. & Jothiprakash, V., 2018. Daily rainfall forecasting for one year in a single run using Singular Spectrum Analysis. *Journal of Hydrology*, 561, 609-621.

Velasco, V.M. & Mendoza, B., 2008. Assessing the relationship between solar activity and some large scale climatic phenomena. *Advances in Space Research*, 42(5), 866-878.

Wilks, D.S., 2019. *Statistical Methods in the Atmospheric Sciences*. 4th Edition, Elsevier.

von der Heydt, A.S., Ashwin, P., Camp, C.D. et al., 2021. Quantification and interpretation of the climate variability record, *Global and Planetary Change*, 197, 1-20.

Xu, J. and Powell, A.M., 2013. What happened to surface temperature with sunspot activity in the past 130 years?. *Theoretical and Applied Climatology*, 111, 609-622.

Yilmaz, E., Akdi, Y., Ugurca, E et al., 2021. Precipitation cycles in Turkey. *Theoretical and Applied Climatology*, 143, 1299-1314.

Zhai, Q., 2017. Influence of solar activity on the precipitation in the North-central China. *New Astronomy*, 51, 161-168.

Zhang, L., Liu, Y., Zhan, H. et al., 2021. Influence of solar activity and EI Nino-Southern Oscillation on precipitation extremes, streamflow variability and flooding events in an arid-semiarid region of China. *Journal of Hydrology*, 601, 126630.

Zhang, X., Xu, Y., Hao, F. et al., 2019. Hydrological components variability under the impact of climate change in a semi-arid river basin. *Water*, 11(6), 1122.